Spontaneous biaxial pattern generation and autonomous wetting switching on the surface of gold/shape memory polystyrene bilayer

Yingzhi Liu[a], Haibao Lu[a,*], Ben Bin Xu[b], David Hui[c] and Yong Qing Fu [b,*]

[a] Science and Technology on Advanced Composites in Special Environments Laboratory, Harbin Institute of Technology, Harbin 150080, China

[b] Smart materials and surfaces lab, Faculty of Engineering and Environment, University of Northumbria, Newcastle upon Tyne, NE1 8ST, UK

[c] Composite Material Research Laboratory, Department of Mechanical Engineering, University of New Orleans, LA 70148, USA

* Corresponding author, E-mail: luhb@hit.edu.cn and richard.fu@northumbria.ac.uk

Abstract

In this paper, shape memory effect induced initiation and evolution of surface patterns (wrinkles and cracks) were studied on the surface of gold/shape memory polystyrene (PS) bilayer, alongside with their impacts on autonomous surface wetting effects. Surface wrinkling was generated as a result of in-plane compression in the gold film where the thermal-induced shape memory effect occurred on the foundation layer. Cracks were generated on gold surface when the wrinkle pattern was further developed at a higher strain. The in-plane surface morphological bifurcation was observed when the crack patterns were developed perpendicular to the wrinkles direction, which is induced by biaxial stress transformation within the gold thin film because of the lateral Poisson's effect. The experimental mechanics investigations describe the relationships

of the initiation/evolvement of surface morphology upon gold/shape memory PS bilayer with respects to various settings, such as the thicknesses of gold films, the applied strain on polymer layer, etc. The associated impact on surface wetting condition brought by the generated biaxial pattern on gold surface was studied. The water contact angle fluctuates within a narrow range according to the pre-strain for the samples after heating under the same plasma treatment times, which indicates that the biaxial pattern (cracks and wrinkles) in this paper have a little effect on the hydrophobicity of the gold film surface when the heated samples were treated by plasma for same times. After the surface plasma treatment, the surface hydrophilicity of the samples after post-annealing is significantly higher than that of the sample after deposition. And the contact angle decreases steadily as the air plasma treatment time is increased, the controllable surface hydrophobicity of gold coated PS bilayer can be achieved by tuning the plasma treatment time.

Keywords: thin film; polystyrene; wrinkle; crack; shape memory polymer

1. Introduction

Elastic instability induced surfaces structural transformations, associating with the energetic switching of the metastable state of elastic substrate under compression/stretching, have been recognized as an effective strategy to achieve diverse patterned surfaces. Based on these, numbers of potential applications have been exploited, such as electronic devices, sensors, hydrophobicity, elastomeric optics and actuators [1-10]. As one of the representative smart materials, shape memory polymers

(SMPs) could add extra values to the smart technologies with their programmable shape changing characteristics, high responsively to the stimuli, large deformation, as well as the intrinsic giant module switching between the glassy state and rubber state [11-15]. The shape memory effect (SME) is the most typical characteristic of the SMPs and can be triggered by heating, electric field and solvent [16-24].

The compressive stress is exerted on the film in an autonomous manner induced by shape memory effect (SME) of substrate. Thus, it is able to trigger a thermal expansion mismatch between the film and the substrate [25-28], and form wrinkling patterns. Cracks were generated parallel to the pre-stretching direction induced by the lateral Poisson's effect which causes a uniaxial tensile stress perpendicular to the pre-stretching direction in the film [29]. Cracks have been known as a kind of mechanical failure mode in engineering applications. Therefore, engineers and researchers usually try to avoid it from happening by taking various measures. Recently, researchers start to take the advantages of the cracks and investigate the mechanics of the films under the formation of microstructures such as surface wrinkles and cracks [30, 31]. Among all these attempts, there remains a challenge on how to generate switchable biaxial patterns on a bilayer system in an autonomous and controllable manner.

Surface wettability is critical for numerous applications in self-cleaning, anti-contamination, micro-fluidics, lab-on-chip devices and biomedical substrates [6, 32-36]. Changing the chemical composition and the geometric structure of the surface are effective approach to tune the surface wettability [37-42]. The limited attempts can be found on the related subject of surface wettability on SMP materials. The recent

study of wetting property on SMP by Lv and co-workers [43], revealed an interesting strategy of realizing a super-hydrophobic surface with self-healing property by employing a mixing technique with design and oxygen plasma treatment. To achieve switchable wetting on the SMP surface could be promising as SMP could enable an autonomous switching of the associated surface morphology.

In this work, we develop a simple strategy to autonomously change the wetting property of the gold/PS bilayer surface, achieve the patterned surfaces by spontaneously forming bi-axial wrinkle and cracks patterns. Surface plasma treatment of the gold coated PS substrate was used to improve the wetting performance of the surface. An experimental study was carried by considering the effects of films thickness and pre-strains applied to the surface patterns. Subsequently, surface wettability of the gold coated PS substrates was studied and plasma treatment on the surface of gold coated PS substrates was performed to study the contact angles evolution.

2. Experimental details

Polystyrene (PS) SMP with a glass transition temperature (T_g) of 60°C was used in this work. The mixed precursor solution (with curing agent) was cast into a Teflon mold, cured at 75°C for 24 hours in the oven. The PS polymer sheets with a thickness of ~ 2 mm were achieved. The sample preparation was carried at room temperature of about 23°C by cutting PS sheets into the rectangular samples with the lateral dimension of $40\,mm \times 10\,mm$. Both ends of the samples were clamped with a customized tensile vise. The gauge length was initially set as 20 mm. The sample was heated to 85ºC and

uniformly stretched using the holder into different strains, 0%, 5%, 10%, 20% and 30%. Then it was cooled down to the room temperature to fix the pre-strain in the PS. Gold film was coated on pre-stretched PS substrates by sputter coating. The thicknesses of gold film were controlled by setting different coating durations, and measured using a profilometer (DEKTAK XT). Subsequently, the samples were placed in the oven and baked at 85°C for 5 minutes and then cooled down to room temperature so that the PS substrate could retrieve its original shape. The surface patterns were observed using a NIKON LV-100 up the right optical microscope.

To examine the effects of film thickness and pre-strain on the surface morphologies, two experiments (each with three groups of samples) were performed. Firstly, gold films with different thicknesses (8 nm, 15 nm and 25 nm) were deposited on pre-stretched PS substrate with 5% pre-strain. Secondly, gold films with the thickness of 25 nm were deposited on pre-stretched PS substrate with different pre-strains (0%, 5 %, 10%, 20% and 30%).

In order to investigate the influence of plasma treatment for the surface wettability, the samples (gold films with the thickness of 25 nm were deposited on pre-stretched PS substrate with different pre-strains) before heating and after heating were further treated in a plasma chamber with an oxygen/nitrogen ratio of 0.2 for different durations and the contact angle of water droplets on the surface of gold film was measured using a drop shape analyzer (Kruss). The conditions of the samples after deposition and the samples after post-annealing were considered. The samples above mentioned were cut into two pieces, that is, there are 6 samples to treat by plasma for different durations. The static

water contact angles along the pre-strain were collected both with drop volumes of 3 μL. The average of five measurements was taken as contact angle for every sample.

3. Results and discussion

3.1 Shape memory induced surface wrinkling

Fig. 1 presents the surface wrinkle morphology (induced by the shape memory effect) of gold/PS bilayer with different thicknesses of gold films and 5% pre-stretched PS after heating. Wrinkle textures which are perpendicular to the direction of pre-strain can be identified on the surface of all these samples. The stored strain energy generated by pre-stretching was released during the heating, resulting in the production of shape recovery and a uniaxial compressive stress in the PS substrate. In this experiment, gold film remained its confinement sate on the PS substrate through testing. Thus a uniaxial compressive stress was generated in the gold film, which can be used to account for the wrinkles appeared on the surface. From Fig. 1, it is clear that the density of wrinkles decreases and wrinkles become more apparent with an increase in the thicknesses of gold films.

Previously, a linear buckling theory has been adopted to predict the critical wavelength of the wrinkles induced by a stiff film buckling on a compliant substrate. It can be expressed as [25, 44]

$$\lambda_c = 2\pi t_f \left[\frac{\left(1-\upsilon_s^2\right)E_f}{3\left(1-\upsilon_f^2\right)E_s} \right]^{1/3} \approx 2\pi t_f \left(\frac{E_f}{3E_s} \right)^{1/3} \tag{1}$$

Where E and υ are Young's modulus and Poisson's ratio, respectively. The subscripts

of f and s represent the film and the substrate, respectively. t_f is the thickness of gold film. The Poisson's ratio and the applied strain are neglected in the Eq. 1, meaning that the critical wavelength is independent of the applied strain. In practice, however, it is necessary to take the material or geometrical nonlinearity into considerations. Therefore, a new theory taking account of the finite and large deformations and geometrical nonlinearities was established to predict the buckling behavior of a stiff film coated on a compliant substrate. The critical wavelength of the wrinkles can be calculated using [2, 45]

$$\lambda = \frac{\lambda_c}{(1+\varepsilon_{pre})(1+\eta)^{1/3}} \tag{2}$$

$$\eta = \frac{5\varepsilon_{pre}(1+\varepsilon_{pre})}{32} \tag{3}$$

The average wavelengths of the wrinkles were evaluated by using Eq. 2 with the mechanical properties of gold film (E_f=78 GPa , $\upsilon_f = 0.42$) and PS substrate (E_s=2.5 MPa , $\upsilon_f = 0.5$ at high temperature above T_g) [26]. Fig. 2 plots the wrinkle wavelength versus the thickness of gold film which was calculated by Eq. 2 and the experimental data, respectively. As shown in Fig. 2, the wrinkle wavelength increases linearly as the thicknesses of gold films increase. The curve of linear fitting is following the results predicted by the theory.

3.2 Formation of complex surface pattern on gold/PS bilayer

The evolution of patterns on gold surface was characterized for the gold film with the thickness of 25 nm coated onto the PS substrate with different pre-strains varied from 0% to 30% after heating (Fig. 3). It can be found in Fig. 3 (a) that only a large number of

horizontal and vertical cracks are randomly distributed on the surface of sample with 0% pre-strain. Upon heating, PS substrate expands more than gold film since the thermal expansion coefficient of PS substrate is remarkably different from that of the gold film. So the gold film is subjected to an isotropic tensile stress in plane during the heating, which could result in randomly distributed cracks on the surface when this stress exceeds the fracture strength of the gold film.

From Fig. 3 (b) to (e), for the pre-stretched samples after heating, the biaxial patterned surfaces in which wrinkles are aligned perpendicularly to the pre-stretching direction and cracks are developed perpendicularly to the wrinkles are observed. Surface wrinkles perpendicular to the pre-stretching direction are generated as a result of in-plane compression (along the direction of pre-stretch) in the gold film where the pre-strain stored is released by the thermal-induced shape memory effect occurred on the PS substrate at the high temperature. Cracks paralleled to the pre-stretching direction are induced by the biaxial stress transformation within the gold thin film due to the lateral Poisson's effect which causes a uniaxial tensile stress perpendicular to the pre-stretching direction. The in-plane surface morphological bifurcation is developed because the cracks perpendicular to the wrinkles direction occur when this tensile stress exceeds the fracture strength of the gold film. This tensile stress increases with the increase of pre-strain. Consequently, the density of cracks increases progressively while the crack spacing became narrow with the increase of pre-strains.

The average wavelength of wrinkles was calculated using the Eq. 2 and the experimental data, respectively. Fig. 4 shows the plots of wrinkle wavelength versus the

applied pre-strain. As shown in Fig. 4, the wrinkle wavelength calculated from Eq. 2 and the experimental data do not show any significant difference. The slope of the liner fitting line (-0.01479) is approximately zero, which indicates that the average wavelength of wrinkles to remain constant with the pre-strains increased from 5% to 30%. The results reveal that the cracks and pre-strains have negligible effects on the wavelength of wrinkles.

Many researchers have established theories which enable the film fracture strength to be obtained from average crack spacing [30, 31, 46]. These theories can be applied to wrinkling-cracking phenomena induced by depositing metallic thin films onto polymers such as in this study. The average crack spacing can be described by [30, 31, 46]

$$d = \frac{2t_f \sigma^*}{E_s(\varepsilon - \varepsilon^*)} \tag{4}$$

Where σ^* and ε^* are the fracture strength and onset fracture strain of the film, respectively. E_s is Young's modulus of the PS substrate, and t_f is the thickness of the gold film. According to Eq. 4, the crack spacing is linearly proportional to the tensile strain.

The obtained experimental data of the average crack spacing as a function of applied pre-strain are shown in Fig. 5. It is clear that the average crack spacing is linearly decreased with the increase of the pre-strain. Uniaxial compressive strain along the direction of pre-strain was developed in the PS substrate during the shape recovery at a high temperature. Whereas tensile strain was perpendicular to the direction of pre-strain and generated by Poisson's effect of the PS substrate. This tensile strain is $\varepsilon = 0.5\varepsilon_{pre}$ for the PS SMP Poisson ratio of 0.5. In this paper,

the applied pre-strains are in a range from 5% to 30%, and the tensile strains are in a range from 2.5% to 15%. Fig. 6 shows the average crack density plotted against the tensile strain. The Fig. 6 illustrates that there is a linearly increase in the average crack density. Therefore, the fracture strength of the film can be deduced by a linear curve fitting about these results. The fracture strength of the 25 nm gold film was calculated to be 21.54 MPa.

3.3 Surface wettability influenced by the bi-axially patterned surface

Fig. 7 (a) shows the snapshots for the water droplets on the surface of gold films with 25 nm thickness deposited on the PS with 0% pre-strains before heating and after heating for the different plasma treatment times. Fig. 7 (b) represents the evolution of water contact angle with the increase of the plasma treatment times for samples of gold films with 25 nm thickness coated on PS substrates with 0% pre-strain. Fig. 7 (b) indicates that it is possible to achieve the tunable hydrophilicity of the surface by using the plasma treatment. Plasma treatment is often used to change the chemical composition of the surface and to improve the surface wettability [37-39]. As for the samples after deposition, the contact angle reduces from 81° (untreated) to 57° after 30 seconds of plasma treatment. Subsequently, with the further increase of the plasma treatment time, the contact angle only shows a slight decrease to 41°. The surfaces of samples with 0% pre-strain after deposition have no clear patterns, and there no changes of the surface pattern were observed before and after plasma treatment. Therefore, the increase of hydrophilicity is caused by the changes of surface chemical compositions

due to the plasma treatment.

The most significant reduction of the contact angle is achieved for the samples (with a minimum contact angle of 15°) after post-annealing, followed by only 30 seconds of plasma treatment. Many cracks randomly distributed on the surface of the samples after post-annealing (as shown in Fig. 3 (a1)). After plasma treatment, however, the surface hydrophilicity of the samples after post-annealing is significantly higher than that of the sample after deposition. It can be concluded that the combined effect of plasma treatment and surface topography greatly enhances the surface hydrophilicity of the surface.

The effects of the plasma treatment durations and pre-strains on the water contact angle for samples of gold films with 25 nm thickness coated on PS substrates with different pre-strain after heating were investigated, and the results are shown in Fig. 8. The surfaces of samples with 0% pre-strain show many arbitrary distributed cracks (as shown in Fig. 3 (a1)). The surfaces of samples with pre-strain from 5% to 30% exhibit the biaxial patterns in which wrinkles are aligned perpendicularly to the pre-stretching direction and cracks are developed perpendicularly to the wrinkles. And the wavelength of wrinkles and the number of cracks increase linearly with the increase of pre-strain. As is illustrated in the Fig. 8, it can be seen that the water contact angle is hardly changed as the pre-strain increase from 0% to 30% for the samples under the same plasma treatment times. The changes of surface topography induced by different pre-strain in here play a negligible effect on the hydrophobicity of the film

surface when the heated samples were treated by plasma for same times. For the samples with same pre-strain, the water contact angle decreases sharply with the plasma treatment time increased to 30 s. It can be found that the contact angle decreases steadily as the air plasma treatment time is increased, and the hydrophobicity of the film surface can be controlled by tuning the plasma treatment time.

4. Conclusions

The spontaneous generation of bi-axial surface patterns consisting of wrinkles and cracks was achieved upon the gold/PS bilayer. When the SME of PS was triggered by heating, the uniaxial compression stress was generated in the gold film, thus yield a surface wrinkling. Quantitative characterizations of the wrinkle morphology suggested that the wrinkle wavelength increased linearly as the thicknesses of gold films increases. It had also been found that the cracks and pre-strains had insignificant effects on the development of wrinkles. Crack patterns had been observed as they originated and developed in parallel to the pre-stretching direction, which were induced by the lateral Poisson's effect. The lateral morphological bifurcation of surface pattern holds the potential of creating biaxial heterostructure surface. The wetting property was assessed on the biaxial patterned surface. The water contact angle is hardly changed as the pre-strain increase for the samples after heating under the same plasma treatment times. It indicates that the biaxial pattern (cracks and wrinkles) in this paper play a negligible effect on the hydrophobicity of the gold film surface when the heated samples were

treated by plasma for same times. After the surface plasma treatment, the surface hydrophilicity of the samples after post-annealing is significantly higher than that of the sample after deposition. And the contact angle decreases steadily as the air plasma treatment time is increased, the controllable surface hydrophobicity of gold coated PS bilayer can be achieved by tuning the plasma treatment time.

Acknowledgements

The authors acknowledged the financial support from the National Natural Science Foundation of China (NSFC) (Grant No. 11422217, 11672642), Program for New Century Excellent Talents in University (Grant No. NCET-13-0172), Foundation for the Author of National Excellent Doctoral Dissertation of the People's Republic of China (Grant No. 201328) and National Youth Top-notch Talent Support Program. Richard Y.Q. Fu would thanks funding supports from EPSRC funds (EP/P018998/1) and Knowledge Transfer Partnership (KTP010548). Ben Bin Xu would thanks the supports from EPSRC funds (EP/N007921/1, EP/L026899/1), and royal society fund (RG150662).

References

[1] Stafford CM, Harrison C, Beers KL, Karim A, Amis EJ, VanLandingham MR, et al. A buckling-based metrology for measuring the elastic moduli of polymeric thin films. Nat Mater. 2004;3(8):545-50.

[2] Jiang H, Khang DY, Song J, Sun Y, Huang Y, Rogers JA. Finite deformation

mechanics in buckled thin films on compliant supports. Proc Natl Acad Sci USA. 2007;104(40):15607-12.

[3] Khang DY, Rogers JA, Lee HH. Mechanical Buckling: Mechanics, Metrology, and Stretchable Electronics. Adv Funct Mater. 2009;19(10):1526-36.

[4] Yu C, O'Brien K, Zhang Y-H, Yu H, Jiang H. Tunable optical gratings based on buckled nanoscale thin films on transparent elastomeric substrates. Appl Phys Lett. 2010;96(4):041111.

[5] Chen Z, Young Kim Y, Krishnaswamy S. Anisotropic wrinkle formation on shape memory polymer substrates. J Appl Phys. 2012;112(12):124319.

[6] Li Y, Dai S, John J, Carter KR. Superhydrophobic surfaces from hierarchically structured wrinkled polymers. ACS applied materials & interfaces. 2013;5(21):11066-73.

[7] Xu B, Hayward RC. Low‐voltage switching of crease patterns on hydrogel surfaces. Adv Mater. 2013;25(39):5555-9.

[8] Xu B, Chen D, Hayward RC. Mechanically gated electrical switches by creasing of patterned metal/elastomer bilayer films. Adv Mater. 2014;26(25):4381-5.

[9] Lee WK, Engel CJ, Huntington MD, Hu J, Odom TW. Controlled Three-Dimensional Hierarchical Structuring by Memory-Based, Sequential Wrinkling. Nano Lett. 2015;15(8):5624-9.

[10] Xu BB, Liu Q, Suo Z, Hayward RC. Reversible Electrochemically Triggered Delamination Blistering of Hydrogel Films on Micropatterned Electrodes. Adv

Funct Mater. 2016;26(19):3218-25.

[11] Lendlein A, Jiang HY, Jünger O, Langer R. Light-induced shape-memory polymers. Nature. 2005;434(7035):879-82.

[12] Behl M, Razzaq MY, Lendlein A. Multifunctional Shape‐Memory Polymers. Adv Mater. 2010;22(31):3388-10.

[13] Lu H, Lei M, Zhao C, Yao Y, Gou J, Hui D, et al. Controlling Au electrode patterns for simultaneously monitoring electrical actuation and shape recovery in shape memory polymer. Compos Part B: Eng. 2015;80:37-42.

[14] Zhao Q, Qi HJ, Xie T. Recent progress in shape memory polymer: New behavior, enabling materials, and mechanistic understanding. Prog Polym Sci. 2015;49:79-120.

[15] Hager MD, Bode S, Weber C, Schubert US. Shape memory polymers: Past, present and future developments. Prog Polym Sci. 2015;49:3-33.

[16] Liu Y, Boyles JK, Genzer J, Dickey MD. Self-folding of polymer sheets using local light absorption. Soft matter. 2012;8(6):1764-69.

[17] Lu H, Yao Y, Huang WM, Leng J, Hui D. Significantly improving infrared light-induced shape recovery behavior of shape memory polymeric nanocomposite via a synergistic effect of carbon nanotube and boron nitride. Compos Part B: Eng. 2014;62:256-61.

[18] Lu H, Yao Y, Huang WM, Hui D. Noncovalently functionalized carbon fiber by grafted self-assembled graphene oxide and the synergistic effect on polymeric shape memory nanocomposites. Compos Part B: Eng. 2014;67:290-5.

[19] Lu H, Liang F, Yao Y, Gou J, Hui D. Self-assembled multi-layered carbon nanofiber nanopaper for significantly improving electrical actuation of shape memory polymer nanocomposite. Compos Part B: Eng. 2014;59:191-5.

[20] Xiao R, Guo J, Safranski DL, Nguyen TD. Solvent-driven temperature memory and multiple shape memory effects. Soft matter. 2015;11(20):3977-85.

[21] Lu H, Wang X, Yao Y, Gou J, Hui D, Xu B, et al. Synergistic effect of siloxane modified aluminum nanopowders and carbon fiber on electrothermal efficiency of polymeric shape memory nanocomposite. Compos Part B: Eng. 2015;80:1-6.

[22] Lu H, Yu K, Huang WM, Leng J. On the Takayanagi principle for the shape memory effect and thermomechanical behaviors in polymers with multi-phases. Smart Mater Struct. 2016;25(12):125001.

[23] Lu H, Yin J, Xu B, Gou J, Hui D, Fu Y. Synergistic effects of carboxylic acid-functionalized carbon nanotube and nafion/silica nanofiber on electrical actuation efficiency of shape memory polymer nanocomposite. Compos Part B: Eng. 2016;100:146-51.

[24] Lu H, Lu C, Huang WM, Leng J. Quantitative separation of the influence of copper (II) chloride mass migration on the chemo-responsive shape memory effect in polyurethane shape memory polymer. Smart Mater Struct. 2016;25(10):105003.

[25] Kim YY, Huang Q, Krishnaswamy S. Selective growth and ordering of self-assembly on metal/polymer thin-film heterostructures via photothermal modulation. Appl Phys Lett. 2010;96(12):123116.

[26] Zhao Y, Huang WM, Fu YQ. Formation of micro/nano-scale wrinkling patterns atop shape memory polymers. J Micromech Microeng. 2011;21(6):067007.

[27] Sun L, Zhao Y, Huang WM, Purnawali H, Fu YQ. Wrinkling Atop Shape Memory Materials. Surf Rev Lett. 2012;19(02):1250010.

[28] Zhao Y, Huang WM, Wang CC. Thermo/chemo-responsive shape memory effect for micro/nano surface patterning atop polymers. Nanosci Nanotechnol Lett. 2012;4(9):862-78.

[29] Chen YC, Crosby AJ. High aspect ratio wrinkles via substrate prestretch. Adv Mater. 2014;26(32):5626-31.

[30] Chung JY, Lee JH, Beers KL, Stafford CM. Stiffness, strength, and ductility of nanoscale thin films and membranes: a combined wrinkling-cracking methodology. Nano Lett. 2011;11(8):3361-65.

[31] Lee J-H, Chung JY, Stafford CM. Effect of Confinement on Stiffness and Fracture of Thin Amorphous Polymer Films. ACS Macro Letters. 2012;1(1):122-6.

[32] Li XM, Reinhoudt D, Crego-Calama M. What do we need for a superhydrophobic surface? A review on the recent progress in the preparation of superhydrophobic surfaces. Chem Soc Rev. 2007;36(8):1350-68.

[33] Zorba V, Stratakis E, Barberoglou M, Spanakis E, Tzanetakis P, Anastasiadis SH, et al. Biomimetic Artificial Surfaces Quantitatively Reproduce the Water Repellency of a Lotus Leaf. Adv Mater. 2008;20(21):4049-54.

[34] Jung YC, Bhushan B. Wetting Behavior of Water and Oil Droplets in

Three-Phase Interfaces for Hydrophobicity/philicity and Oleophobicity/philicity. Langmuir. 2009;25(24):14165-73.

[35] Samuel B, Zhao H, Law K-Y. Study of Wetting and Adhesion Interactions between Water and Various Polymer and Superhydrophobic Surfaces. The Journal of Physical Chemistry C. 2011;115(30):14852-61.

[36] Han Y, Liu Y, Wang W, Leng J, Jin P. Controlled wettability based on reversible micro-cracking on a shape memory polymer surface. Soft Matter. 2016;12(10):2708-14.

[37] Gou HL, Xu JJ, Xia XH, Chen HY. Air plasma assisting microcontact deprinting and printing for gold thin film and PDMS patterns. ACS applied materials & interfaces. 2010;2(5):1324-30.

[38] Zhu X, Zhang Z, Men X, Yang J, Xu X, Zhou X. Plasma/thermal-driven the rapid wettability transition on a copper surface. Appl Surf Sci. 2011;257(8):3753-7.

[39] Lee WK, Engel CJ, Huntington MD, Hu J, Odom TW. Controlled Three-Dimensional Hierarchical Structuring by Memory-Based, Sequential Wrinkling. Nano Lett. 2015;15(8):5624-29.

[40] Yao Y, Wei H, Wang J, Lu H, Leng J, Hui D. Fabrication of hybrid membrane of electrospun polycaprolactone and polyethylene oxide with shape memory property. Compos Part B: Eng. 2015;83:264-9.

[41] Yao Y, Li J, Lu H, Gou J, Hui D. Investigation into hybrid configuration in electrospun nafion/silica nanofiber. Compos Part B: Eng. 2015;69:478-83.

[42] Mittal V, Saini R, Sinha S. Natural fiber-mediated epoxy composites – A review. Compos Part B: Eng. 2016;99:425-35.

[43] Lv T, Cheng Z, Zhang E, Kang H, Liu Y, Jiang L. Self-Restoration of Superhydrophobicity on Shape Memory Polymer Arrays with Both Crushed Microstructure and Damaged Surface Chemistry. Small. 2017;13(4).

[44] Li JJ, An YH, Huang R, Jiang HQ, Xie T. Unique aspects of a shape memory polymer as the substrate for surface wrinkling. ACS Applied Materials Interfaces. 2012;4(2):598-03.

[45] Yang S, Khare K, Lin P-C. Harnessing Surface Wrinkle Patterns in Soft Matter. Adv Funct Mater. 2010;20(16):2550-64.

[46] Chen ZB. Self-assembly of Nanopatterns on Shape Memory Polymer Substrates. ProQuest LLC: Northwestern University; 2015.

Figure captions:

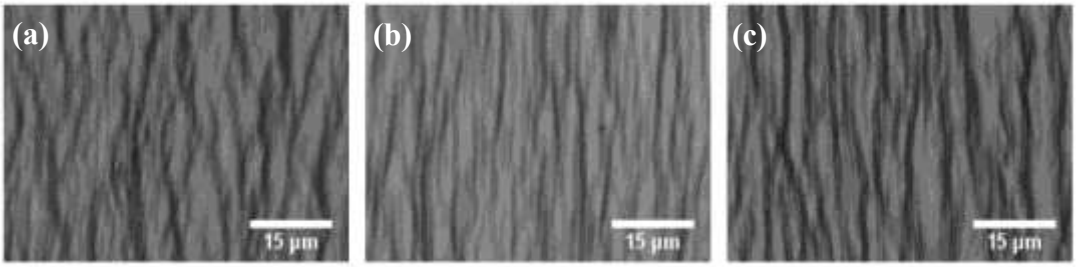

Fig. 1. Optical micrographic images of shape memory induced wrinkling on gold/PS with various thicknesses of gold films (a) 8 nm, (b) 15 nm, (c) 25 nm and 5% pre-stretched PS after heating

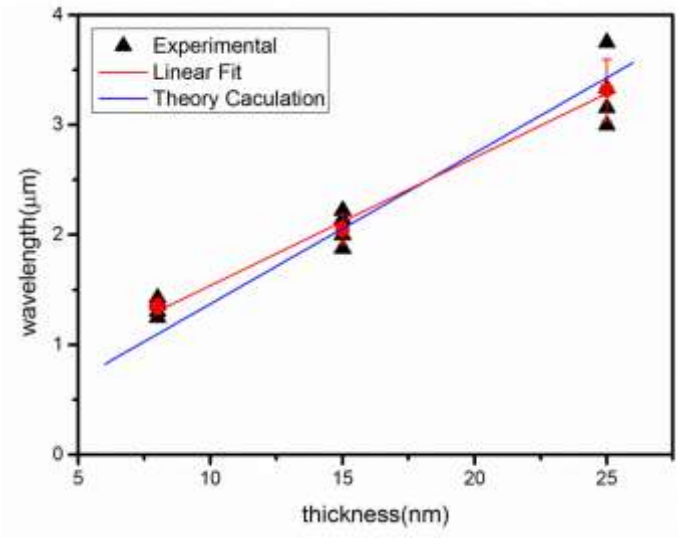

Fig. 2. The average wavelength of the wrinkles versus the thickness of gold film.

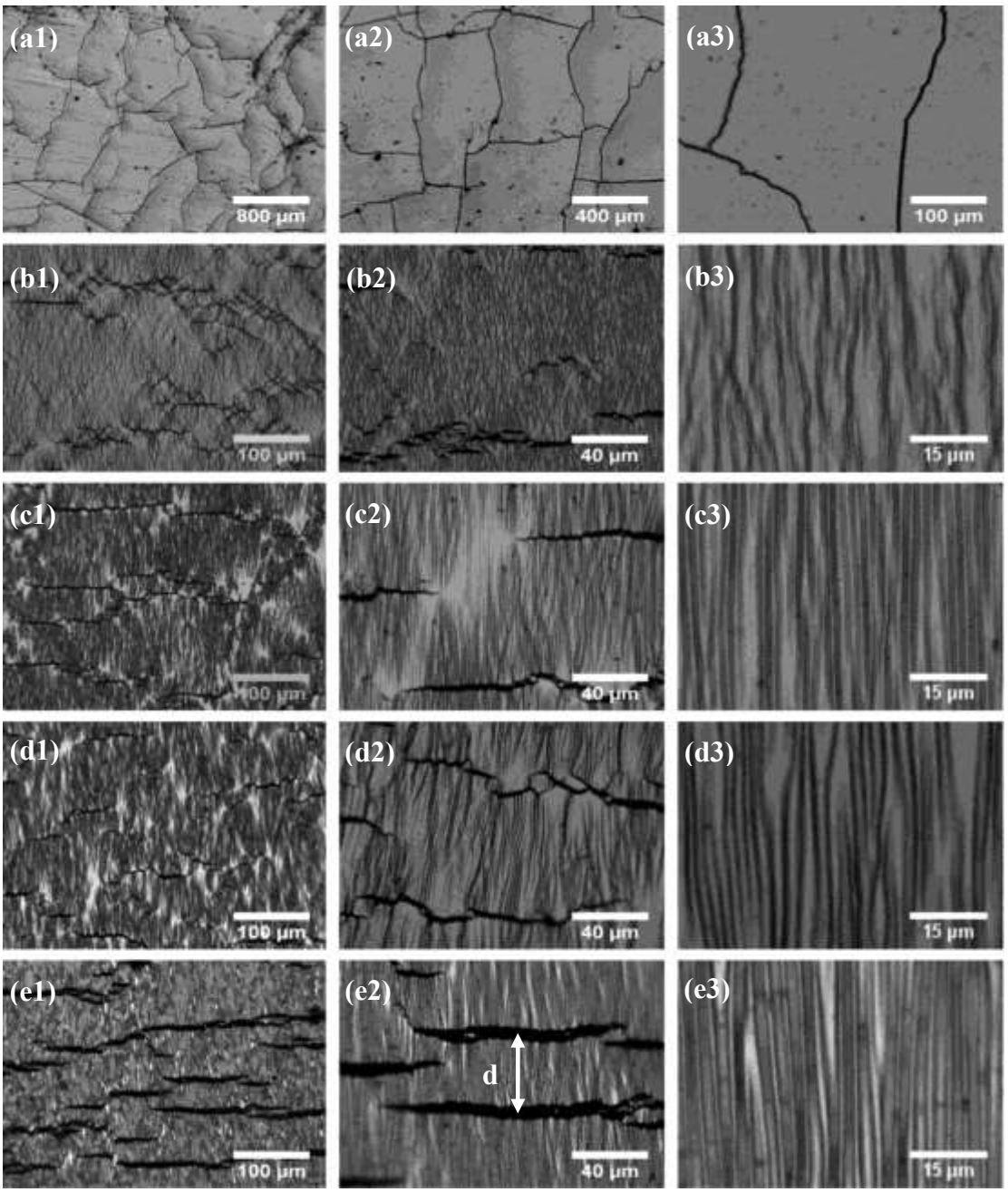

Fig. 3. Optical micrographic images of the occurrence of surface pattern on gold/PS bilayer with (a) 0%, (b) 5%, (c) 10%, (d) 20%, (e) 30% pre-strain. And the thickness of gold film is 25 nm.

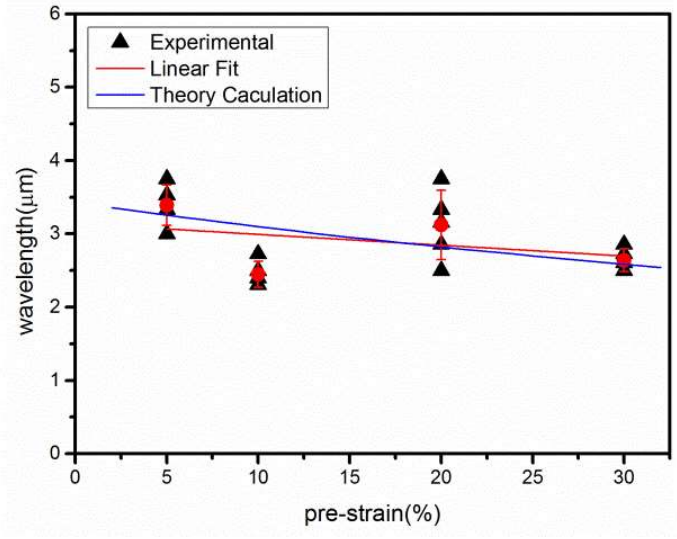

Fig. 4. The average wavelength of the wrinkles versus the applied pre-strain.

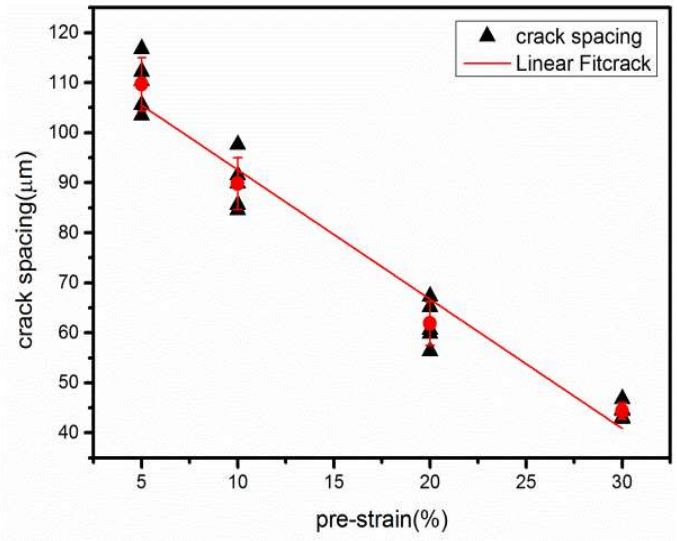

Fig. 5. The average crack spacing versus the applied pre-strain.

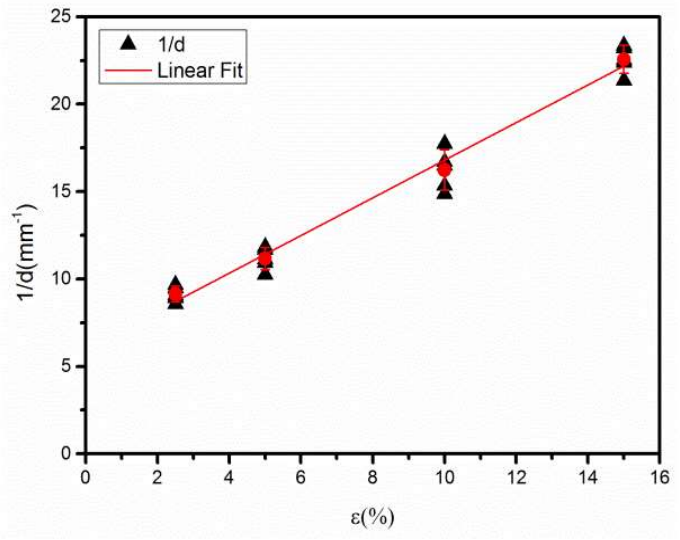

Fig. 6. The average crack density versus the tensile strain.

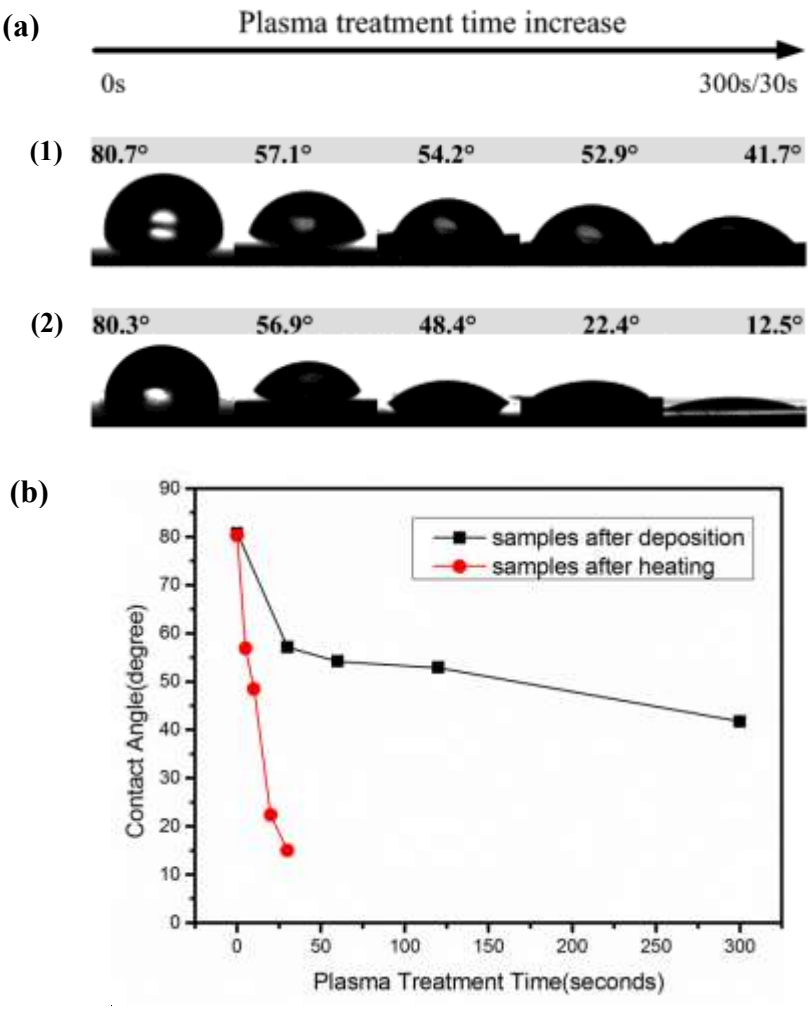

Fig. 7. (a) Snapshots for the water droplets on the surface of gold coated PS after (1) deposition; (2) post-annealing for different plasma treatment times. (b) Water contact angles versus plasma treatment time.

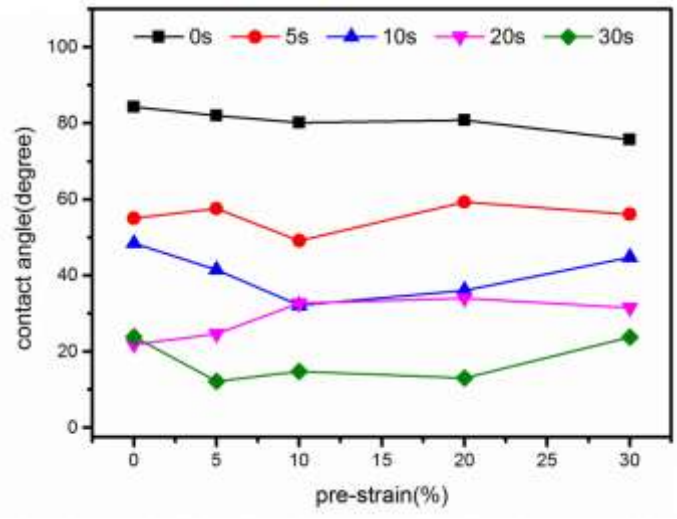

Fig. 8. Water contact angle versus pre-strain under the different plasma treatment times.